# Velocity and pressure field correlation analysis for low-order modeling of elbow flow

Andre Baramili, Ludovic Chatellier, Laurent David, Loïc Ancian

# Velocity and pressure field correlation analysis for low-order modeling of elbow flow

**A. BARAMILI[a,b], L. CHATELLIER [b], L. DAVID [b], L. ANCIAN[a]**

a. VIBRATEC SA - F69134 Ecully Cedex, France.
andre.baramili@vibratec.fr, loic.ancian@vibratec.fr
b. Institut P', Univ. de Poitiers - ENSMA, F86961 Futuroscope Chasseneuil Cedex, France.
ludovic.chatellier@univ-poitiers.fr, laurent.david@univ-poitiers.fr

## Résumé :

*Les écoulements de liquides fortement turbulents dans des réseaux de tuyauterie peuvent constituer une source permanente de sollicitation dynamique de la structure, ce qui peut à son tour mener à la rupture par fatigue. Dans le but final de produire un modèle réduit de l'excitation induite par l'écoulement, la présente étude évalue la corrélation entre pression et vitesse dans l'écoulement en coude. Avec une méthodologie du type LES précédemment validée, une simulation de l'écoulement d'eau au passage d'un coude à 90° et nombre de Reynolds 5.6 x $10^5$ a produit un ensemble de réalisations du champ local de vitesse et pression. La corrélation entre les champs de pression et vitesse sont étudiées. La Décomposition Orthogonale aux Valeurs Propres (POD) des champs de vitesse est appliquée sous la forme de Snapshot-POD pour retrouver des structures cohérentes de l'écoulement. Enfin, le champ de pression est projeté sur les modes de l'écoulement (POD étendue) et une discussion sur la construction d'un modèle réduit de l'excitation basé sur les modes étendus est proposée.*

## Abstract:

*The highly turbulent flow of liquids in piping systems can constitute a steady-state source of dynamic loading of the structure, which might in turn lead to fatigue failure. As part of an effort to build a reduced-order model of the flow-induced excitation, the present study analyzes the correlation found between pressure and velocity in the elbow flow. A previously validated incompressible Large-eddy simulation (LES) of water flowing at Reynolds number 5.6 x $10^5$ through a 90° elbow was used to provide a series of realizations of the local velocity and pressure fields. The correlation between pressure and the velocity fields is evaluated. Proper Orthogonal Decomposition (POD) of the velocity field is applied under the form of Snapshot-POD, giving coherent flow motion information. The pressure field is finally projected onto the flow modes (extended POD) and a discussion regarding the construction of a low-order model of the excitation based on the extended modes is proposed.*

**Key words: Fluid-structure interaction, Turbulence induced vibration, reduced-order modeling, POD.**

# 1 Introduction

The highly turbulent flow of dense fluids through piping systems singularities dynamically excites the structure by means of an unsteady pressure field originated at the flow and transferred to the pipe walls. The flow-induced excitation is broadband and most significant in the low-frequency range, which makes it dangerous to thin-walled structures and may eventually lead to fatigue failure. In order to evaluate the spatial distribution of the flow-induced excitation over a small curvature radius elbow, Nakamura *et al.* [1] placed 124 pressure transducers on the elbow, upstream and downstream of it. The wall pressure measurements for Reynolds numbers of order $10^6$ seem to indicate that the most energetic excitation takes place downstream of the intrados, where the flow separates. Ebara *et al.* [2] and Yamano *et al*. [3] also used multiple pressure transducers and identified pressure peaks at specific non-dimensional frequencies. Takamura *et al.* [4] associate these characteristic frequencies with three oscillating flow structures formed on the elbow intrados: the separation region, vortex shedding in the separation region and two counter-rotating vortices formed on the bend and convected downstream of it, known as the Dean Vortices (Dean [5]). These vortices share the cross-section of the pipe and dominate one another alternately, in a mouvement named Swirl-Switching, which is also a typical oscillatory motion found in the elbow flow.

These coherent flow structures formed on the elbow have been extensively studied, both numerically (Rütten *et al.* [6], *Eguchi et al.* [7], Dutta and Nandi [8]) and experimentally (Tunstall and Harvey [9], Ono *et al.* [10], Vester *et al.* [11], Sakakibara and Machida [12]). Nevertheless, few studies have analyzed the relationship between the coherent motions of the velocity field and the resulting pressure distribution. Indeed, these large-scale motions generally contain most of the flow kinetic energy, allowing for the simpler reconstitution of the dynamic system by means of low-order modeling. Moreover, information on the dynamic load applied by the fluid on the structure may be extracted from flow reduced-order models. Techniques based on the orthogonal decomposition of the flow field provide an orthogonal base of flow modes as a function of their contribution to the total kinetic energy of the system (Lumley, [13]). This can be done with a sufficiently high number of uncorrelated realizations of the local velocity field, a technique known as *Snapshot*-POD [14]. When the pressure field is projected onto the POD modes of the fluid, the extended modes (*e-POD,* [15]) couple pressure and velocity information that can be useful in the construction of a model of the flow-induced dynamic excitation.

Incompressible Large-Eddy Simulations (LES) of water flowing at Reynolds number $5.6 \times 10^5$ through a 90° elbow were used to evaluate the correlation between pressure and velocity in the elbow flow. Section 2 of this article describes the numerical approach used for the unsteady flow computation and underlines the principle of the statistical tools to be applied to the snapshot data thereby issued. Section 3 illustrates the correlation between the flow and the pressure field on multiple sections of the elbow, followed by the evaluation of the POD and e-POD modes present in the flow. Section 4 discusses the modeling of the flow dynamic loading using coupled pressure and velocity modes and finally presents the conclusion of this study and future perspectives.

# 2 Materials and Methods

## 2.1 Elbow Flow Simulation

A Reynolds Averaged Navier Stokes (RANS) and a Large-Eddy Simulation (LES) of water flowing at Reynolds number 5.6 x $10^5$ through a 90° elbow were performed using StarCCM+ (CD-Adapco$^R$). The fluid domain was an elbow with curvature radius $\gamma = 1.5D$ where $D = 99.4\ mm$ is the duct diameter; the bend is preceded by a straight section of length $2D$ and followed by another straight section $4D$ long. The tridimensional mesh was generated following two steps: first, a prism layer was generated close to the wall and then a polyhedral mesh filled up the pipe core. The prism layer was 20 mm thick and contained 49 sublayers piled up along the wall's normal direction; each sublayer was 1.15 thicker than the previous one (closer to the wall) resulting in a first cell centered at a dimensionless wall distance $y^+ \leq 1$. For the polyhedral mesh in the pipe core, a target cell size of 5 mm was chosen, resulting in a final mesh count of 570 000 cells.

The RANS incompressible steady simulation was first performed in order to initialize the turbulence over the fluid domain. On the duct walls, the no-slip velocity condition was imposed whereas the outlet boundary condition was of pressure outlet type. Velocity inlet was chosen for the inflow boundary situated $2D$ upstream of the bend entrance. In order to correctly simulate a completely developed turbulent duct flow at the entrance of the elbow, velocity, turbulent intensity and turbulent length scale profiles were measured using PIV and injected in the inlet of the RANS simulations.

The LES was then performed on the converged solution of the steady simulations, keeping the boundary conditions unchanged. Unsteady wall-bounded turbulence was generated using the Synthetic Eddy Method described by Jarrin *et al.* [16]. Second-order time discretization with a time step of 5 x $10^{-4}$ ensured a Current Flow Number (CFL) inferior to one, taking into account the smallest size cell found in the fluid domain and the highest flow speed calculated by the RANS simulation. The Smagorinsky Subgrid Scale approach was used to model the small scales of turbulence that are not directly resolved by the LES. The equation of state was set up to consider a constant density liquid; the Segregated Flow Model was used so that the three components of velocity and the pressure were calculated separately (see Demirdžić and Muzaferija [17] for details on the Segregated Model). 20 seconds of the solution were calculated; pressure and the three components of velocity were extracted at a sampling frequency of 100 Hz from all cells contained in the each of the five reference planes illustrated in Figure 1.

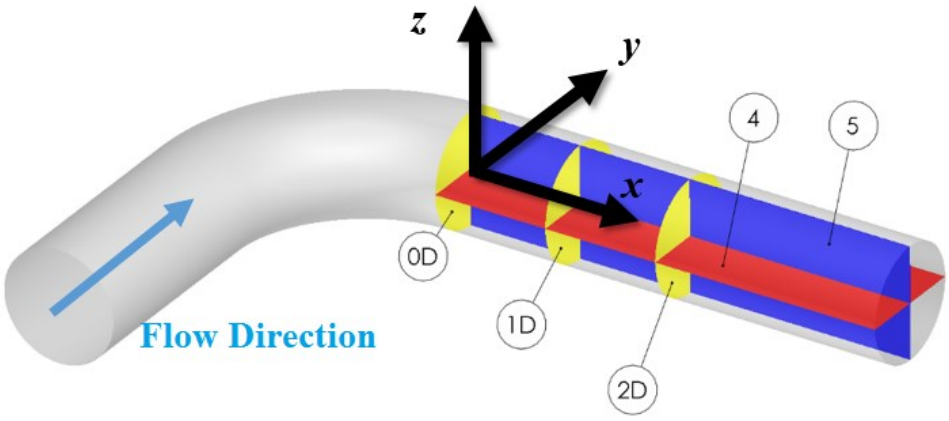


*Figure 1 - Reference planes where snapshots were taken.*

## 2.2 Proper Orthogonal Decomposition

The POD is a linear method consisting in the determination of an orthogonal and ordinated base that optimally approximates data known from a large dimension set. In fluid mechanics, the POD application results in the identification of the flow structures that have the largest least square projection on the velocity field. Let us call $u_i(\boldsymbol{x}, t)$ a set of realizations of the velocity field and $\boldsymbol{\Phi}(\mathbf{x}, \mathrm{t})$ the flow structures modal base. Mathematically, one seeks to maximize the expression:

$$\frac{\langle (\boldsymbol{u}, \boldsymbol{\Phi})^2 \rangle}{(\boldsymbol{\Phi}, \boldsymbol{\Phi})}$$

with $\langle \cdot \rangle$ the ensemble average and $(\boldsymbol{u}, \boldsymbol{\Phi})$ the scalar product of $\boldsymbol{u}$ and $\boldsymbol{\Phi}$. This maximization problem corresponds to the solution of the integral Eigen value problem:

$$\int_{\mathcal{D}} \mathcal{R}_{ij}(\boldsymbol{x}, \boldsymbol{x}') \phi_j^{(n)}(\boldsymbol{x}') d\boldsymbol{x}' = \lambda_n \phi_i^{(n)}(\boldsymbol{x})$$

where $\lambda_n$ is the n$^{\text{th}}$ Eigen value and represents the amount of energy contained in the Eigen vector $\phi_i^{(n)}(\boldsymbol{x})$, which follows a decreasing order (the first mode is the most energetic). $\mathcal{R}_{ij}$ is the spatial correlation tensor, also known as the two-point correlation function over the physical domain $\mathcal{D}$:

$$\mathcal{R}_{ij} = \langle \boldsymbol{u}(\boldsymbol{x}, t)\, \boldsymbol{u}^*(\boldsymbol{x}', t) \rangle$$

The projection of the velocity field onto the Eigen vector basis results in the POD coefficients, $a_n(t)$. These coefficients contain the temporal evolution of the Eigen spatial vectors in the reconstruction of the velocity field dynamics. The POD contribution consists in this reconstruction which can be made using only the most important modes (the $N_{POD}$ first modes), a process known as truncation, as follows:

$$a_n(t) = \int_{\mathcal{D}} \boldsymbol{u}_i(\boldsymbol{x}, t) \phi_i^{(n)}(\boldsymbol{x}) d\boldsymbol{x}$$

$$\boldsymbol{u}_i(\boldsymbol{x}, t) = \sum_{n=1}^{\infty} a_n(t) \phi_i^{(n)}(\boldsymbol{x}) \approx \sum_{n=1}^{N_{POD}} a_n(t) \phi_i^{(n)}(\boldsymbol{x})$$

This approach involving the two-point correlation function is not always applicable when the flow data is produced by numerical simulation, where there might be poor temporal resolution whereas the data is generally very richly resolved spatially. Sirovich [14] proposed the replacement of the two-point correlation function by a matrix of temporal correlations. Consider a set of $M$snapshots containing information of the velocity at $N$ points such that $M \ll N$. The time lapse between two consecutive snapshots, $\tau$, is large enough so that the velocity data on both are uncorrelated. If $\boldsymbol{u}(\boldsymbol{x}, t_i)$ is the set of $M$ realizations of the flow that constitute the snaphot base ($i = 1, \ldots, M$) and $\boldsymbol{\phi}$ an Eigen function issued by the POD, one may write:

$$\boldsymbol{\phi}(\boldsymbol{x}) = \sum_{k=1}^{M} A_k \boldsymbol{u}(\boldsymbol{x}, t_k)$$

where $A_k$ is the vector of time coefficients. It is possible to show that the POD coefficients can be calculated from a matrix of temporal correlation $\boldsymbol{C}$ defined as the internal product of the velocity vectors over the domain Ɗ at times *k* and *i*, as follows:

$$\sum_{k=1}^{M} C_{ki}A_k = \lambda A_i \;; \quad \boldsymbol{C} = C_{ki} = \frac{1}{M}(\boldsymbol{u}(\boldsymbol{x}', t_k), \boldsymbol{u}(\boldsymbol{x}', t_i)), \quad i = 1, \dots, M.$$

From the Correlation Matrix $\boldsymbol{C}$ an orthogonal ordinated set of Eigen vectors ($\boldsymbol{\phi}$) and Eigen values ($\lambda_n$) can be directly calculated using a matrix diagonalization technique called Singular Value Decomposition (SVD, [18]).

## 2.3 Extended-POD

The POD is currently a well accepted and widely applied tool for retrieving coherent structures in turbulent flows and hence analyzing large amounts of experimental or numerical data on a great number of complex flow configurations. Borée [15] proposed an extension of the POD modes to consider the correlation between the velocity field and any other physical quantities of flow, such as temperature, concentration or pressure. Knowing that the random time coefficients are uncorrelated among themselves ($\langle a_n a_p \rangle = \lambda_n \delta_{np}$), the averaged projection of the velocity field on them can be rewritten taking into account the orthogonal decomposition of the velocity field, as follows:

$$\langle a_p \boldsymbol{u}(\boldsymbol{x}) \rangle = \langle a_p \sum_n a_n \boldsymbol{\phi}^n(\boldsymbol{x}) \rangle = \sum_n \langle a_n a_p \rangle \boldsymbol{\phi}^n(\boldsymbol{x}) = \lambda_p \boldsymbol{\phi}^p(\boldsymbol{x})$$

Therefore, the POD modes can be written:

$$\boldsymbol{\phi}^p(\boldsymbol{x}) = \frac{\langle a_p \boldsymbol{u}(\boldsymbol{x}) \rangle}{\lambda_p}$$

Let $P(\boldsymbol{x})$ be a set of realizations of the pressure field that correspond one by one with a realization of the velocity field $\boldsymbol{u}(\boldsymbol{x})$. The orthogonal modes extended to the pressure are retrieved from a projection of the pressure field on the random time coefficients of the POD:

$$\boldsymbol{\psi}^p(\boldsymbol{x}) = \frac{\langle a_p P(\boldsymbol{x}) \rangle}{\lambda_p}$$

The velocity modes extended to the pressure therefore carry information on how correlated are the coherent flow structures in respect to the resulting pressure field. Another way to assess this correlation is to directly compute the correlation coefficient between the pressure and the velocity signals. The Person's Product defines the correlation between a pressure signal at a point $\alpha$ and a velocity signal at point $\beta$ and reads:

$$\Upsilon_{P_\alpha u_{i,\beta}} = \frac{cov(P_\alpha(t), u_{i,\beta}(t))}{\sigma_{P_\alpha} \sigma_{u_{i,\beta}}}$$

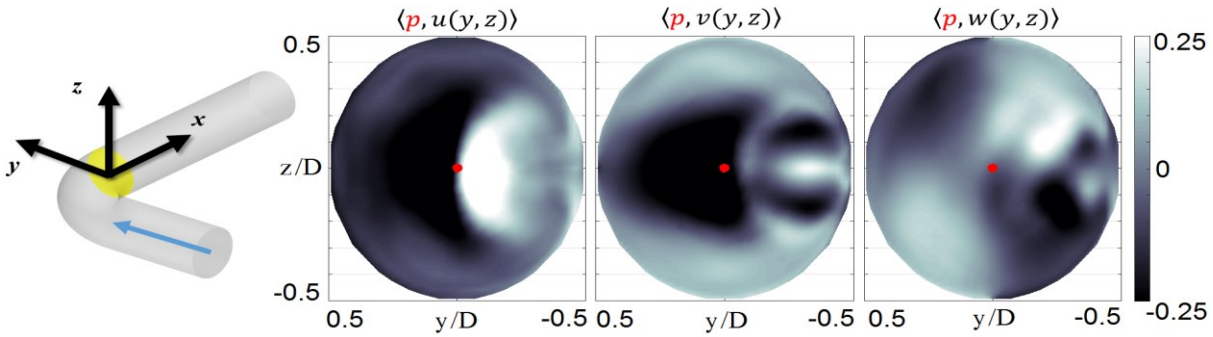


*Figure 2 - Correlation between pressure (on red dot) and each component of velocity on Section 0D. The blue arrow indicates flow direction.*

Here, $\sigma_{P_\alpha}$ and $\sigma_{u_{i,\beta}}$ are respectively the standard deviations of the pressure and the velocity signals.

# 3 Results

Three main flow structures are formed in the elbow flow (for more details, see [4, 6, 7, 10]), namely, the flow separation on the elbow intrados, the vortex shedding from this region and finally the Dean Vortices. These large scale motions have an oscillatory behavior and the pressure field originating there is likely to interact with the duct's wall.

Figure 2 illustrates the correlation charts of the pressure signal at a point located in the middle of Section 0D (red dot) and the velocity signals for every other point in this section and for each of the three components $u$, $v$ and $w$. The correlations of the pressure with the axial component ($u$) are the strongest compared to the other velocity components; the chart pictures a high correlation region in the center of the pipe and low correlation towards the walls. The correlations of the $v$ component on the contrary are concentrated in the outer part of the section and seem to translate the impact of the separation on the intrados region (to the right), where a pocket of positive correlation is observed inside a zone of strong negative correlation. For each component there seems to exist a vertical symmetry, considering the horizontal center line; for $u$ and $v$, the signal of correlation is maintained, whereas for $w$ the signal is inversed between the upper and lower parts of the section.

A similar behavior is observed at the Section 1D, mainly when evaluating the correlations of the pressure in the intrados (right side of the duct), as shown in Figure 3. Additionally, the separation at the interior of the elbow is clearly pictured by the correlations with the $u$ and $v$ components. The Dean Vortices are strongly present at this section as can be seen in the correlations with the $v$ and $w$ components, where

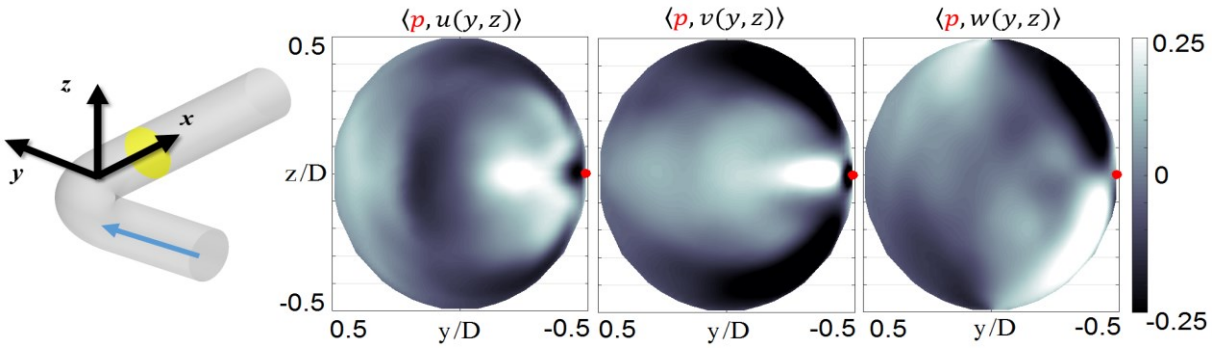


*Figure 3 - Correlation between pressure (on red dot) and each component of velocity on Section 1D. The blue arrow indicates flow direction.*

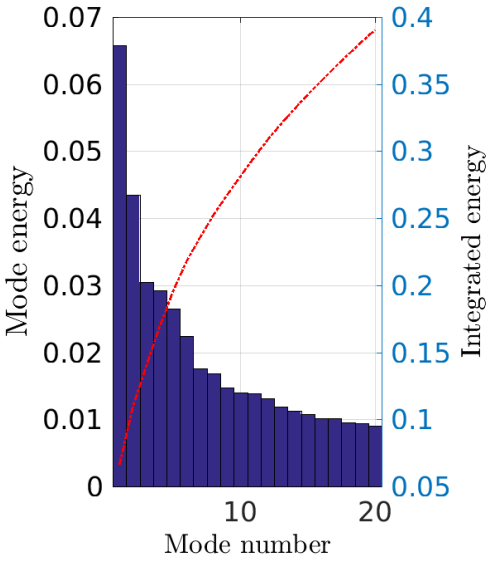


*Figure 4 - Energy distribution according to mode number. Blue bars, left axis: percentage of energy contained in each mode; red line, right axis: cumulated percentage of energy.*

regions of high positive and negative correlations are formed in both upper and bottom parts; again, the signs are inversed across the symmetry line for the $w$ component, differentiating it from the two others.

The POD analysis was then performed over 2.000 velocity snapshots taken at each of the five sections shown in Figure 1. For a correct decomposition of the velocity field, ergodicity must be respected, which means that the number of samples must be large enough to ensure that the flow dynamics are well represented. For this purpose, a convergence analysis was performed on the snapshots obtained by the LES simulation. This analysis consisted in computing the Root Mean Square (RMS) value of the velocity fluctuations over multiple points of Section 4 as a function of the number of samples taken into account. When the RMS values reach a steady position, one may infer that the number of samples is enough to satisfy the ergodicity condition. For this study, convergence was reached with around 1.000 samples of the velocity field.

The Eigen values produced by the POD are a measure of the kinetic energy of the flow contained by each mode. Figure 4 illustrates the kinetic energy distribution of the orthogonal modes of the velocity field. The blue bars represent the percentage of energy in each mode ($\varepsilon_i = \lambda_i / \sum_{j=1}^{N} \lambda_j$) and the red line

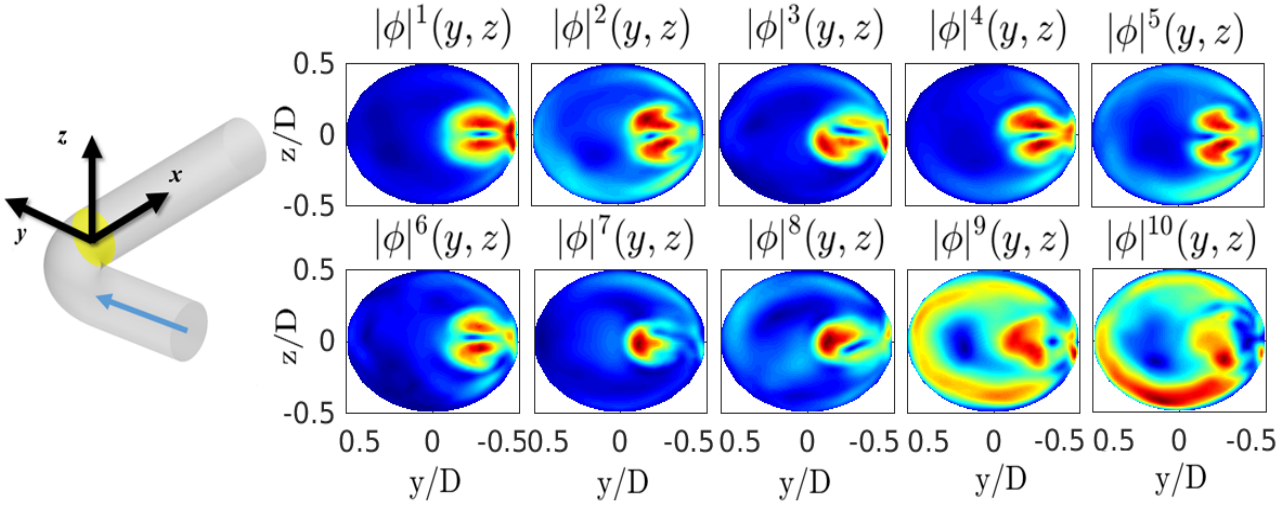


*Figure 5- Ten first POD modes of the velocity magnitude over section 0D. Blue arrow indicates flow direction. Intrados is on the right.*

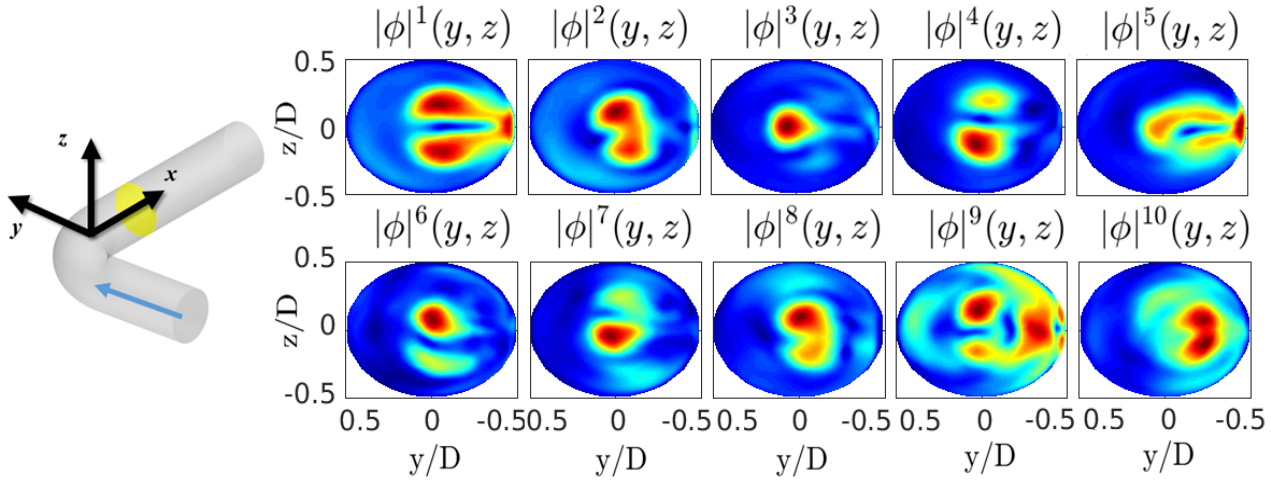


*Figure 6- Ten first POD modes of the velocity magnitude over section 1D. Blue arrow indicates flow direction. Intrados is on the right.*

traces the cumulated sum. All five sections were considered in the same decomposition and therefore the total kinetic energy is not limited to any of the sections separately. This is one of the reasons why the first and most energetic mode contains only 6.5% of the total kinetic energy of the system, and the first 20 modes' energies cumulated barely reach 40%. Moreover, the flow is highly tridimensional, making it less likely for planar modes to represent the system's dynamics.

Figures 5 to 7 picture the ten most energetic modes of the velocity magnitude ($\sqrt{u^2+v^2+w^2}$) over the cross-sections 0D, 1D and 2D. The color levels are arbitrary as to emphasize the mode shapes. On Section 0D (Figure 5), the modes are often characterized by the presence of lobe shaped regions close to the elbow intrados (right part of the section). This recurrence indicates that the separation is captured by most of the illustrated modes and seems to dominate the flow dynamics at this section located in the exit of the elbow. Modes 9 and 10 start to show the presence of a circular structure towards the outer wall. In Section 1D (Figure 6), the lobe regions are translated towards the duct's center and assume a more circular shape. Most of the modes are quasi-symmetric with respect to the horizontal centerline.

However, some of the asymmetric modes seem to encounter a symmetric partner, as is the case for mode 4 and mode 6. This behavior is an evidence of the oscillatory movement of the Dean Vortices, which dominate alternately one another with one situated in the upper part of the section and the other situated in the lower part. Figures 8 and 9 picture the POD modes of the magnitude of velocity at sections 4 and

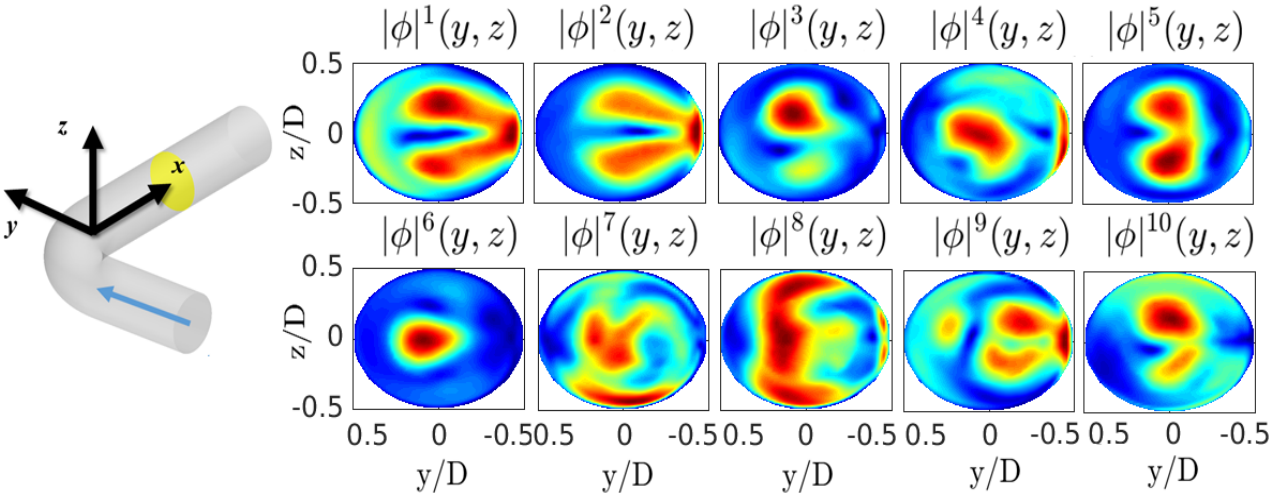


*Figure 7- Ten first POD modes of the velocity magnitude over section 2D. Blue arrow indicates flow direction. Intrados is on the right.*

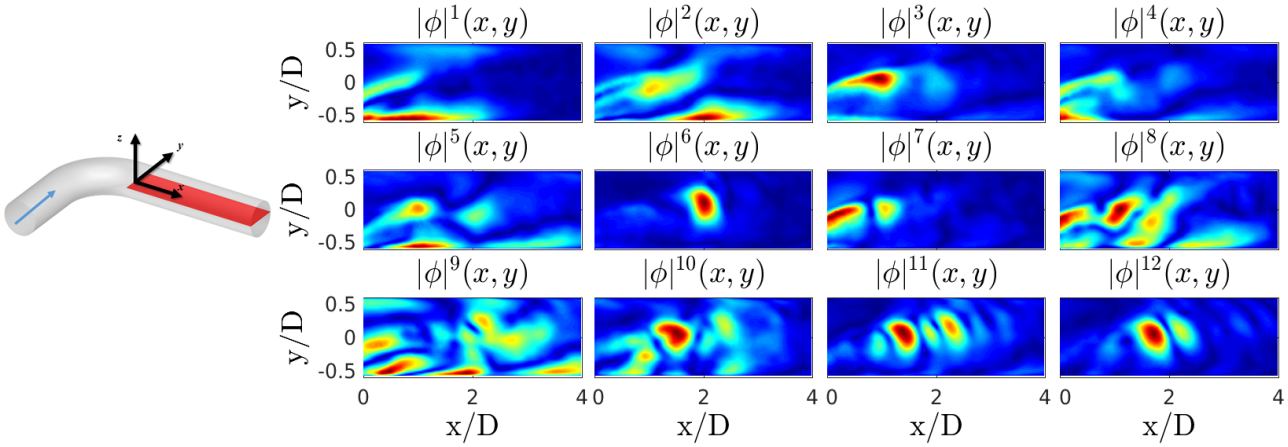


*Figure 8 – Twelve first POD modes of the velocity magnitude over section 4. Blue arrow indicates flow direction.*

5. Section 4 (Figure 8) contains a clear view of the separation on the intrados and the vortex shedding originated on this region. Once again, one can notice that separation seems to dominate the shapes of the first 5 modes whereas the vortex shedding structure is more present from the 6th mode on.

Finally, Figure 9 pictures the POD modes of the 5th and last section. The first mode clearly shows the presence of the Dean Vortices, developed at the elbow curvature on its exit and convected downstream of it. Modes 2, 5, 8 and 9, for instance, picture the interaction of different flow structures such as the Dean Vortices and the vortex shedding originated in the separation region; they are often quasi-symmetric within the boundaries of the section. For the purpose of clarity, figures 5 to 9 illustrate the POD modes unweighted regarding their relative energy contribution (Figure 4).

The fluctuating pressure field was then projected onto the POD modes of the magnitude of velocity at the five reference planes, resulting in the extended modes illustrated in figures 10 to 14. On Section 0D all ten first extended modes present high positive and negative values close to the intrados region, with generally two lobes symmetrically placed with respect to the horizontal centerline, but with inversed signs. Modes 4 and 6 are almost perfectly symmetric, whereas modes 3 and 7 present approximately the same shape with inversed sign.

The shape symmetry between the upper and lower halves is a trend observed in all extended modes, even if in some of them the signs are inversed whereas in others the symmetry is complete. At Section 1D (Figure 11), the circular regions of high correlation move towards the center of the pipe or, when

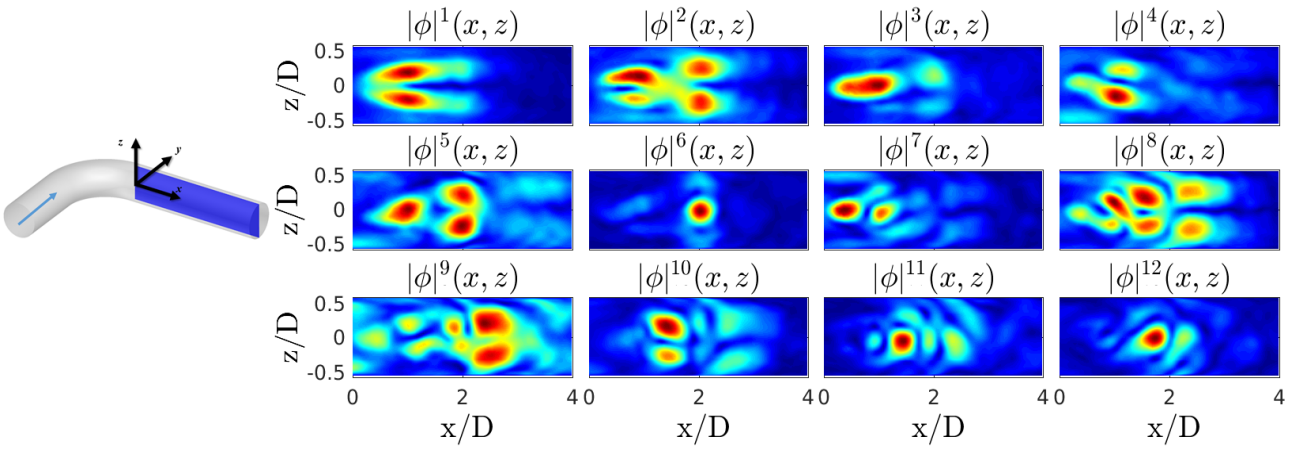


*Figure 9 – Twelve first POD modes of the velocity magnitude over section 5. Blue arrow indicates flow direction.*

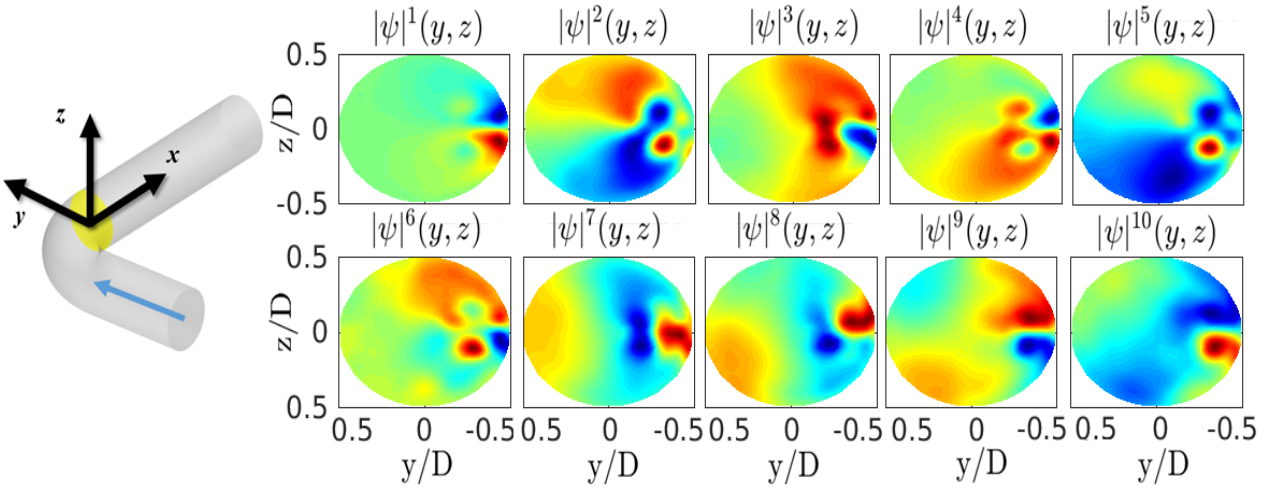


*Figure 10 - Ten first extended POD modes over section 0D. Blue arrow indicates flow direction. Intrados is on the right.*

there are more than one, to the center of the upper or lower half. They also tend to spread, finally occupying the whole surface of the section as they move towards Section 2D (Figure 12).

When in Section 0D the symmetry axis is well-defined and coincides with the centerline, in sections 1D and 2D it tilts to different angles, if it exists at all, depending on the extended mode studied. Also, moving downstream and far from the separation zone, the mode shapes start to look more like monopole, dipole and even quadrupole sources. The mode's evolution as they move downstream is best noticed when observing their projection on sections 4 and 5 (figures 13 and 14, respectively).

The four first extended modes in Section 4, where separation is clearly seen, indicate that the oscillation of the separation region along the $y$ direction has a great impact on the local pressure field. Modes 1 to 4 present a symmetric behavior along the $z$ direction and with respect to the pipe centerline (see Figure 14), with an inversion of the correlation signs in some cases. Further extended modes indicate that the pressure travels downstream in an alternate movement of a rib-like shape characterized by one region of positive correlation followed by a region of negative correlation. Regarding the extended mode shapes it can be assumed that the extent of the influence of the separation region on the pressure field is limited to about $1.5D$ downstream from the elbow exit and that, from this point on, the Dean Vortices and the vortex shedding are the coherent structures with greatest impact. Again, for the sake of clarity, the extended modes were plotted with arbitrary color levels and are not weighted.

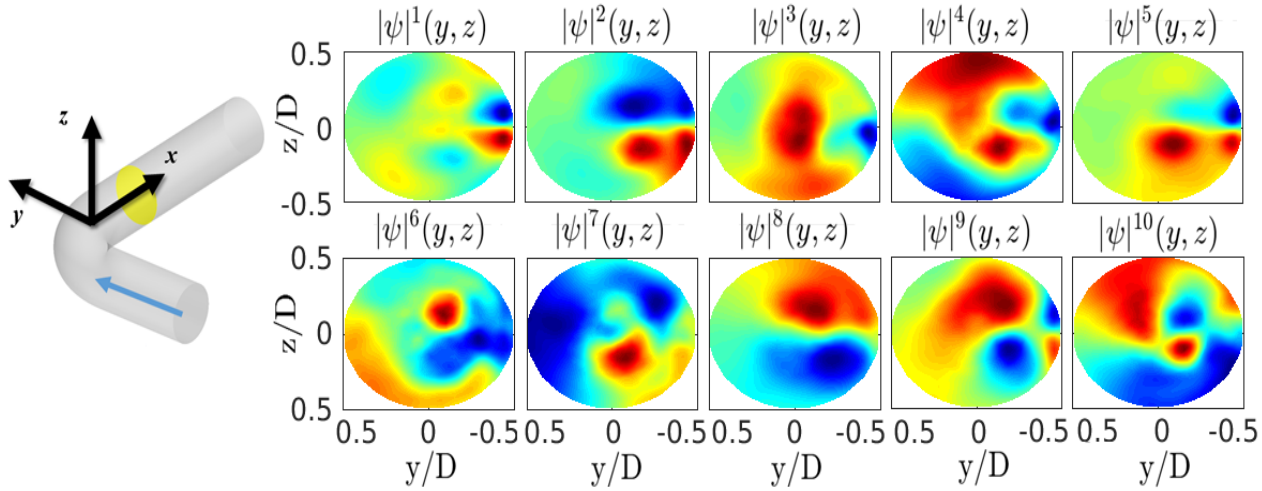


*Figure 11 - Ten first extended POD modes over section 1D. Blue arrow indicates flow direction. Intrados is on the right.*

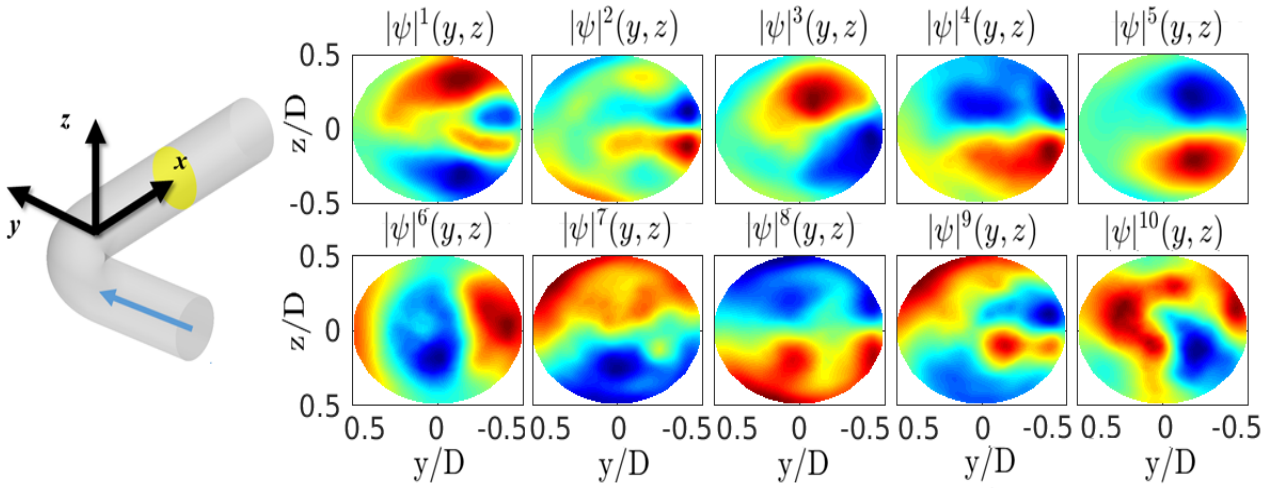


*Figure 12 - Ten first extended POD modes over section 2D. Blue arrow indicates flow direction. Intrados is on the right.*

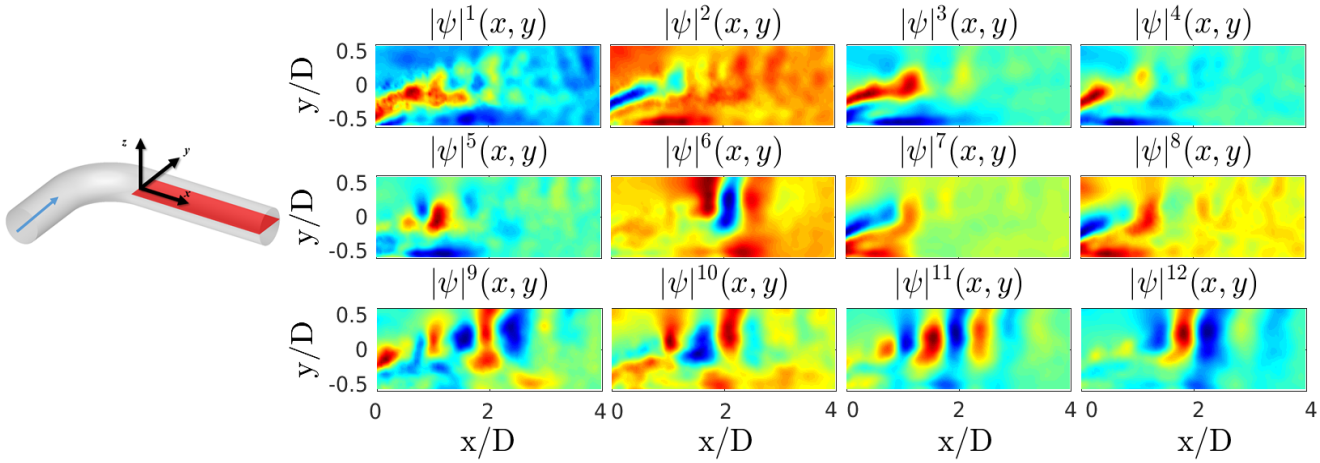


*Figure 13 - Twelve first extended POD modes over section 4. Blue arrow indicates flow direction.*

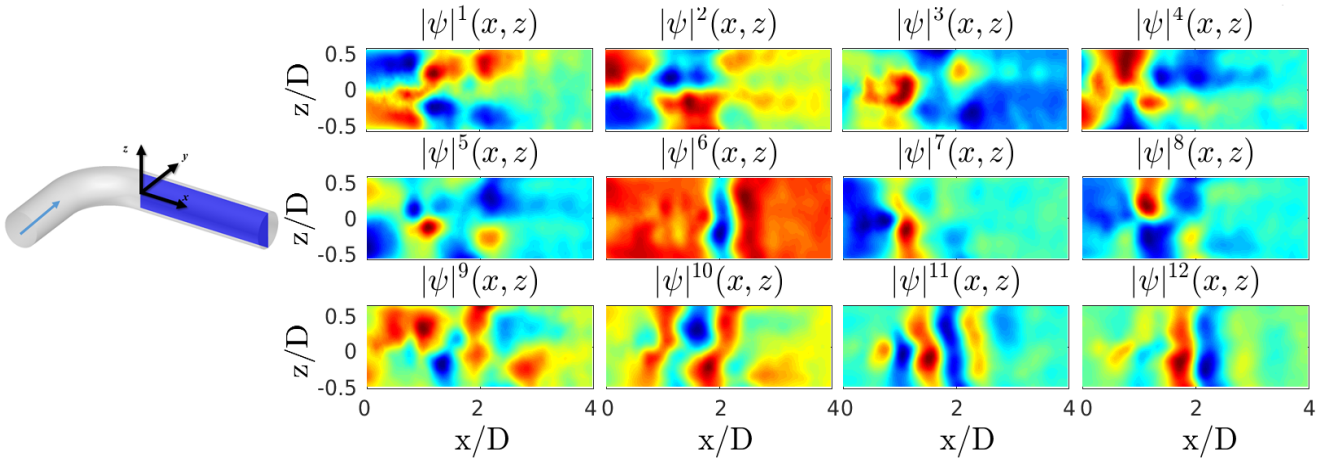


*Figure 14 - Twelve first extended POD modes over section 5. Blue arrow indicates flow direction.*

# 4 Discussion and conclusions

A Large-Eddy Simulation of the turbulent flow of water through a 90° elbow was used to produce a large amount of velocity and pressure field data over multiple plane sections on the elbow. This data was extracted under the form of snapshots in a number large enough to ensure the ergodicity condition. POD and extended POD were applied to the data in order to obtain information on the coherent flow structures and their influence on the local pressure field. The LES data correctly captured the typical coherent structures identified in the literature concerning elbow flow; as for the kinetic energy content, more than 20 modes are needed to provide 40% of the total energy of the tridimensional flow over the entire simulated domain. The projection of the pressure field onto the POD modes revealed interesting features regarding the correlation of the coherent flow structures and the dynamic excitation of the duct walls. Even if the numerical data was originally obtained with an incompressible LES, the extended modes often present source-like shapes.

As remarked by Ukeiley *et al.* [19], coherent motions may be used to build reduced-order models of the dynamics of complex turbulent flows, namely using the technique of *Galerkin-POD*. The present study shows that the elbow flow can be modeled using POD modes, even if more than a few are needed to capture most of its kinetic energy. It was also shown that information on the pressure field dynamics can be retrieved from the POD modes. Future work will consist in collecting experimental coupled data on the velocity field, pressure fluctuations on the duct walls and the structural vibration, with the goal of building a low-order model to link all three of them.

# 5 References

[1] T. Nakamura, T. Shiraishi, Y. Ishitani, H. Watakabe, H. Sago, T. Fujii, A. Yamaguchi and M. Konomura, "Flow-Induced Vibration of a Large-Diameter Elbow Piping Based on Random Force Measurement Caused by Conveying Fluid: Visualization Test Results," *ASME 2005 Pressure Vessels and Piping Conference,* pp. 457-463, 2005.

[2] S. Ebara, Y. Aoya, T. Sato, H. Hashizume, Y. Kazuhisa, K. Aizawa and H. Yamano, "Pressure Fluctuation Characteristics of Complex Turbulent Flow in a Single Elbow With Small Curvature Radius for a Sodium-Cooled Fast Reactor," *Journal of Fluids Engineering,* vol. 132, no. 11, p. 111102, 2010.

[3] H. Yamano, M. Tanaka, N. Kimura, H. Ohshima, H. Kamide and O. Watanabe, "Development of flow-induced vibration evaluation methodology for large-diameter piping with elbow in Japan sodium-cooled fast reactor," *Nuclear Engineering and Design,* vol. 241, no. 11, pp. 4464-4475, 2011.

[4] H. Takamura, S. Ebara, H. Hashizume, K. Aizawa and H. Yamano, "Flow visualization and frequency characteristics of velocity fluctuations of complex turbulent flow in a short elbow piping under high Reynolds number condition," *Journal of Fluids Engineering,* vol. 134, no. 10, p. 101201, 2012.

[5] W. Dean, "Note on the motion of fluid in a curved pipe," *The London, Edinburgh, and Dublin Philosophical Magazine and Journal of Science,* vol. 4, no. 20, pp. 208-223, 1927.

[6] F. Rütten, W. Schröder and M. Meinke, "Large-eddy simulation of low frequency oscillations of the Dean vortices in turbulent pipe bend flows," *Physics of Fluids,* vol. 17, no. 3, p. 035107, 2005.

[7] Y. Eguchi, T. Murakami, M. Tanaka and H. Yamano, "A finite element LES for high-Re flow in a short-elbow pipe with undisturbed inlet velocity," *Nuclear Engineering and Design,* vol. 241, no. 11, pp. 4368-4378, 2011.

[8] P. Dutta and N. Nandi, "Effect of Reynolds Number and Curvature Ratio on Single Phase Turbulent Flow in Pipe Bends," *Mechanics and Mechanical Engineering,* vol. 19, no. 1, pp. 5-16, 2015.

[9] M. Tunstall and J. Harvey, "On the effect of a sharp bend in a fully developed turbulent pipe-flow," *Journal of Fluid Mechanics,* vol. 34, pp. 595-608, 1968.

[10] A. Ono, N. Kimura and A. Tobita, "Influence of elbow curvature on flow structure at elbow outlet under high," *Nuclear Engineering and Design,* pp. 4409-4419, 2011.

[11] A. K. Vester, R. Örlü and P. H. Alfredsson, "POD analysis of the turbulent flow downstream a mild and sharp bend," *Experiments in Fluids,* vol. 56, no. 3, pp. 1-15, 2015.

[12] J. Sakakibara and N. Machida, "Measurement of turbulent flow upstream and downstream of a circular pipe bend," *Physics of Fluids,* vol. 24, no. 4, p. 041702, 2012.

[13] J. L. Lumley, "The structure of inhomogeneous turbulent flows," *Atmospheric turbulence and radio wave propagation,* vol. 790, pp. 166-178, 1967.

[14] L. Sirovich, "Turbulence and the dynamics of coherent structures. Part I: Coherent structures," *Quarterly of applied mathematics,* vol. 45, no. 3, pp. 561-571, 1987.

[15] J. Borée, "Extended proper orthogonal decomposition: a tool to analyse correlated events in turbulent flows," *Experiments in Fluids,* vol. 35, no. 2, pp. 188-192, 2003.

[16] N. Jarrin, S. Benhamadouche, D. Laurence and R. Prosser, "A synthetic-eddy-method for generating inflow conditions for large-eddy simulations," *International Journal of Heat and Fluid Flow,* vol. 27, no. 4, pp. 585-593, 2006.

[17] I. Demirdzic and S. Muzaferija, "Numerical method for coupled fluid flow, heat transfer and stress analysis using unstructured moving meshes with cells of arbitrary topology," *Computer methods in applied mechanics and engineering,* vol. 125, no. 1-4, pp. 235-255, 1995.

[18] G. H. Golub and C. F. Van Loan, Matrix Computation, JHU Press, 2012.

[19] L. Ukeiley, L. Cordier, R. Manceau, J. Delville, M. Glauser and J. Bonnet, "Examination of large-scale structures in a turbulent plane mixing layer. Part 2. Dynamical systems model," *Journal of Fluid Mechanics,* vol. 441, pp. 67-108, 2001.